Ecosystems
https://doi.org/10.1007/s10021-024-00913-0

Linking Post-fire Tree Density to Carbon Storage in High-Latitude Cajander Larch (*Larix cajanderi*) Forests of Far Northeastern Siberia

H. D. Alexander,[1]* A. K. Paulson,[2] M. M. Loranty,[3] M. C. Mack,[4] S. M. Natali,[5] H. Pena,[6] S. Davydov,[7] V. Spektor,[8] and N. Zimov[7]

[1]*College of Forestry, Wildlife, and Environment, Auburn University, Auburn, Alabama 36849, USA;* [2]*Humboldt-Toiyabe National Forest, United States Forest Service, 1200 Franklin Way, Sparks, Nevada 89503, USA;* [3]*Department of Geography, Colgate University, Hamilton, New York 13346, USA;* [4]*Center for Ecosystem Science and Society, Northern Arizona University, 224 Peterson Hall, Flagstaff, Arizona 86011, USA;* [5]*Woodwell Climate Research Center, 149 Woods Hole Road, Falmouth, Massachusetts 02540-1644, USA;* [6]*Department of Forestry, Forest and Wildlife Research Center, Mississippi State University, Starkville, Mississippi 39762, USA;* [7]*Pacific Geographical Institute, Far East Branch, Russian Academy of Sciences, Northeast Science Station, Cherskiy, Republic of Sakha (Yakutia), Russian Federation;* [8]*Melnikov Permafrost Institute, Siberian Branch, Russian Academy of Sciences, Merzlotnaya, 36, Yakutsk, Republic of Sakha (Yakutia), Russian Federation*

Abstract

With climate warming and drying, fire activity is increasing in Cajander larch (*Larix cajanderi* Mayr.) forests underlain by continuous permafrost in northeastern Siberia, and initial post-fire tree demographic processes could unfold to determine long-term forest carbon (C) dynamics through impacts on tree density. Here, we evaluated above- and belowground C pools across 25 even-aged larch stands of varying tree densities that established following a wildfire in ~ 1940 near Cherskiy, Russia. Total C pools increased with increased larch tree density, from ~ 9,000 g C m^{-2} in low-density stands to ~ 11,000 g C m^{-2} in high and very high-density stands, with increases most pronounced at tree densities < 1 stem m^{-2} and driven by increased above- and belowground (that is, coarse roots) and live and dead (that is, woody debris and snags) larch biomass. Total understory vegetation and non-larch coarse root C pools declined with increased tree density due to decreased shrub C pools, but these pools were relatively small compared to larch biomass. Fine root, soil organic matter (OM), and near surface (0–30 cm) mineral soil (MS) C pools varied little with tree density, although soil C pools held most (18–28% in OM and 44–51% in MS) C stored in these stands. Thus, if changing fire regimes promote denser stands, C storage will likely increase, but whether this increase offsets C lost during fires remains unknown. Our findings highlight how post-fire tree demographic processes impact C pool distribution and stability in larch forests of Siberian permafrost regions.

Received 2 November 2023; accepted 14 April 2024

Supplementary Information: The online version contains supplementary material available at https://doi.org/10.1007/s10021-024-00913-0.

Author Contribution HA contributed to conceptualization, methodology, investigation, validation, resources, visualization, supervision, project administration, funding acquisition, writing-original draft, and writing–review editing; AP helped in formal analysis, methodology, and writing—review editing; ML, SN, and MM contributed to conceptualization, methodology, validation, resources, supervision, project administration, funding acquisition, and writing—review editing; HP, SD, VS, and NZ done investigation and writing—review editing.

*Corresponding author; e-mail: heather.alexander@auburn.edu

Published online: 28 May 2024

Key words: wildfire; Russia; permafrost; tree density; tree demographics; C pool; boreal forest.

Highlights

- High tree density led to higher larch tree C pools and lower understory C pools.
- Soil organic matter and near surface mineral soil C pools did not vary with tree density.
- Variation in post-fire tree density impacts long-term C distribution in larch forests

Introduction

Needleleaf, deciduous larch (*Larix* spp.) forests that cover $\sim$ 3 million km^2 across Siberia are a crucial component of the global carbon (C) cycle (Kobak and others 1996; Abaimov 2010; Loranty and others 2016, 2021). These forests lie atop and protect highly vulnerable ice- and C-rich 'yedoma' permafrost, cover > 70% of Siberian continuous permafrost areas, and contain more than one-quarter of permafrost soil C in areas of continuous permafrost (Kharuk and others 2010; Loranty and others 2016; Strauss and others 2017). Larch forest occurrence, regeneration, and persistence are tightly coupled with low-frequency (80—350 year fire rotation interval) fire disturbances, ignited by lightning or humans during the relatively dry growing season (Kharuk and others 2011; Berner and others 2012), that range in severity from surface fires that often leave behind living trees with residual seed crops within the burn perimeter to stand-replacing fires that kill most trees (Kharuk and others 2021). Fires reduce C stocks in larch forests, at least temporarily, by consuming vegetation and organic soils (Kasischke and Stocks 2012), and/or destabilizing permafrost (Holloway and others 2020), creating a pulse of C into the atmosphere, and potentially a positive feedback to climate warming (Witze 2020; Descals and others 2022). Over the post-fire successional interval, however, fires can initiate an array of effects on larch forest recovery that may magnify or offset initial fire effects by influencing net ecosystem C balance, local surface energy dynamics, and future fire potential (Alexander and others 2012a, 2018; Cai and Yang 2016; Kirdyanov and others 2020). Thus, documenting current-day C storage in larch forests is critical for predicting future patterns of global C cycling and feedbacks to the climate system (Fan and others 2023), especially given the recent increase in fire extent, severity, and frequency across Siberia in conjunction with climate warming (Kharuk and others 2021; Descals and others 2022; Talucci and others 2022a).

An important way that increased fire activity can impact larch forest C storage is to alter patterns of tree recruitment during post-fire succession that differs from those of the pre-fire stand. Larch seeds, which are wind-dispersed, do not survive fire and do not form a persistent seedbank (Abaimov 2010); therefore, post-fire recruitment relies on nearby seed sources from mature, seed-bearing trees that avoid or survive fire within the burned area (Talucci and others 2022b) or in nearby unburned stands (that is, biological legacies) (Brown and others 2015). Post-fire environmental conditions within the seedbed and underlying soils and biological interactions among tree recruits and co-occurring organisms (for example, seed predators and soil biota) (Stewart and others 2021; Hewitt and others 2022c) interact to provide ''safe sites'' (Borth and others 2023) and serve as additional filters to determine post-fire tree establishment (Cai and others 2018). Notably, fire severity impacts on the residual depth of soil organic matter (OM) can be a major determinant of soil moisture, temperature, and rooting volume, which impact seed germination and seedling establishment (Johnstone and Chapin III 2006; Alexander and others 2018). Because initial recruitment patterns drive future stand dynamics, fire effects on forest recovery can lead to successional trajectories of varying tree composition and/or density, and in some cases, forest loss (Furyaev and others 2001; Tchebakova and others 2009; Cai and others 2013). For example, larch forests in the northern part of their range are typically monodominant, so changes in tree recruitment can produce forests ranging in structure from open-canopy stands with a well-developed understory of shrubs and grasses to over-stocked, closed-canopy stands with minimal understory development (Kharuk and others 2010; Sofronov and Volokitina 2010). In the southern portion of larch range, relative recruitment of larch compared to co-occurring hardwoods and evergreen conifers can result in forests varying both in tree composition and structure (Furyaev and others 2001). Ultimately, post-fire patterns of forest recruitment unfold as stands mature to impact C storage (Alexander and others 2012; Mack and others 2021) because differences in stand composition and structure drive traits of dominant vegetation in ways that impact the balance between C gains through biomass accumulation and C losses due to

decomposition and subsequent fires (Fan and others 2023).

The primary objectives of this research were to quantify vegetation, detrital (snags and downed woody debris), and soil (OM and near surface mineral (30 cm depth)) C pools across a gradient of Cajander larch (*Larix cajanderi* Mayr.) tree density in northeastern Siberia to better understand how post-fire demographic processes influence C dynamics as stands mature. We focused on even-aged stands on relatively flat topography in the uplands that originated after a single fire ($\sim$ 20 km^2) in $\sim$ 1940 to limit impacts of stand age and/or site conditions on C pools. We hypothesized that increased larch density would increase C stored in larch tree above- and belowground biomass, moss biomass, and organic soils, while decreasing C stored in shrubs, but with no impacts on C pools in underlying surface mineral soils, which would be spatially isolated from aboveground changes in C pools. We also expected more snags and woody debris with increased density due to self-thinning. A better understanding of larch forest C dynamics in response to changing fire behavior with climate warming is critically important for predicting future C trends in these C-rich and highly vulnerable forest ecosystems underlain by continuous permafrost.

Methods

Study Area

Research occurred near the Northeast Science Station (NESS) in Cherskiy, Sakha Republic, Russian Federation in far northeastern Siberia, (68.74° N, 161.40° E), which is located on the Kolyma River, $\sim$ 250 km north of the Arctic Circle and 130 km south of the Arctic Ocean (Fig. 1A). Climate is continental, with annual (1980–2017) mean air temperatures in summer (June–August) and winter (December–February) of 10.9 and − 31.0 °C, respectively, and average annual temperature of − 10.4 °C. Annual average precipitation is low (235 mm y^{-1}), with $\sim$ half falling during summer (Cherskiy Meteorological Station; https://rp5.ru/Weather_archive_in_Cherskiy). Snow commonly covers the ground from October to May, and average depth during those months has gradually increased over time, from 29 cm 1997 to 55 cm in 2017. Soils in the study area are classified as Cambic Turbic Cryosols (Eutric, Nechic, Siltic, Endorelictistagnic Thixotropic) (Fedorov-Davydov and others 2018), according to the World Reference Base (WRB) System (Anjos and others 2016). Carbon-rich, Pleistocene-age yedoma permafrost with high ice content exists in many places across the area (Strauss and others 2017).

Forests in this region of the Russian Far East are typically open-canopy, sparse stands dominated by Cajander larch (Alexander and others 2012a; Berner and others 2012; Loranty and others 2016), a deciduous needleleaf conifer adapted to growth on continuous permafrost and a short, cool growing season (Abaimov 2010). Trees average 4–8 m in height (Alexander and others 2012). Seeds are produced annually, with heavy masts every 2–3 year, no dormancy, and dissemination via wind dispersal beginning in early autumn (Abaimov 2010). Understory vegetation consists of primarily tall (typically $>$ 1 m), mostly deciduous shrubs, short (typically $<$ 1 m tall) shrubs, forbs, grasses, lichens, and mosses (see Paulson and others 2021 for details).

The current fire return interval in the taiga of the Russian Far East is 65–122 years, with an annual burned area of $\sim$ 1.3 Mha y^{-1} in 2020 (Talucci and others 2022a). Most fires occur in larch forests underlain with continuous permafrost, which contain $>$ 50% of total soil (0–1 m depth) C pools found in arctic-boreal permafrost ecosystems (Loranty and others 2016; Talucci and others 2022a). Fire frequency and extent are increasing across the region (Descals and others 2022; Kharuk and others 2021), with $\sim$ 121 million hectares burned in the East Siberia taiga zone from 2001 to 2020 (Talucci and others 2022a). Many fires are surface fires that cause 60–75% stand mortality (Krylov and others 2014; Rogers and others 2015; Shuman and others 2017), largely due to root damage (Sofronov and Volokitina 2010), as larch leaves have a high moisture content that tends to suppress crown fires (Rogers and others 2015). Stand-replacing fires are becoming more frequent (Schaphoff and others 2016), with high severity fires that cause $>$ 80% tree mortality occurring in the eastern larch forests near our study site (Webb and others 2024).

Study Design

To determine if variations in larch tree density impact C storage within above- and belowground C pools, we sampled 25 larch stands ($\sim$ 0.5 ha each, located 0.1–3.0 km apart) from 2010 to 2017 that varied in tree density (0.03–3.70 trees m^{-2}) within a forested area ($\sim$ 20 km^2) that burned in $\sim$ 1940 (Fig. 1B). This forest was $\sim$ 2 km from the NESS and exhibited little elevational variation (23–93 m above mean sea level). Stands varying in density

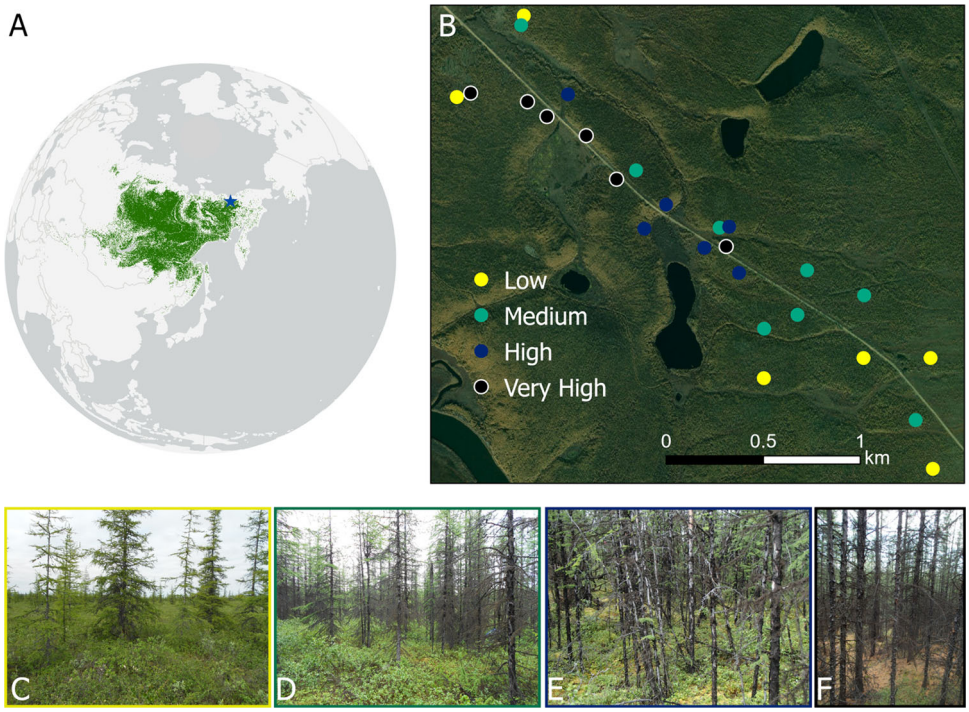

Figure 1. **A** Distribution of larch (*Larix* spp.) forests across permafrost regions of eastern Siberia and study site (blue star) location near Cherskiy, Russia, **B** stand locations within the fire perimeter, which burned in ~ 1940, and example photos of stands of **C** low-, **D** medium-, **E** high-, and **F** very high density.

from low- (trees sparse ''savannah-like'') to very-high (trees so dense crowns were touching each other) (Fig. 1C–F) were identified and selected for sampling using satellite imagery and field reconnaissance. All stands were in the uplands on gradually sloping or flat terrain.

We focused on even-aged stands that originated after a single fire to limit any impacts of stand age and/or site conditions on C pools (Alexander and others 2012a), and we focused on tree density, and not basal area, because density is an indicator of varying levels of post-fire tree recruitment (Alexander and others 2018). Differences in tree density across the fire perimeter likely reflect variations in post-fire seed availability, soil burn severity, and other factors affecting seed germination and seedling survival, such as weather and animal activity (Cai and others 2013, 2018; Alexander and others 2018). Initial levels of larch recruitment following fire typically persist as stands mature because deterioration of the seedbed and competition from other vegetation restrict infilling processes (Alexander and others 2018). Larch establishment in the absence of fire is largely limited to small-scale areas that provide safe sites, such as tip-up mounds (Borth and others 2023). We also noted a low-density of large (> 20 cm DBH), fire-killed (indicated by heavy char) stumps, snags, and coarse woody debris across all stands. Given the very slow decomposition rates in this region, even of small-diameter wood, the evidence of large-diameter trees from the previous stand across the burned area indicates that the pre-burn forest structure was low-density and open-canopied, and that observed density patterns likely emerged after the most recent fire.

We confirmed that stands originated following the same fire and were relatively even-aged, thereby limiting known effects of stand age on C pools (Alexander and others 2012a), by aging 10 randomly-sampled trees from each stand using a wood core or slab obtained from the base (~ 20 to 30 cm from soil surface) of each tree. Wood samples were dried at 60 °C, sanded sequentially with finer grit sizes to obtain a smooth surface, scanned at high-resolution and analyzed for ring count using WinDendro (Regent Instruments, Canada). Tree ring counts for all trees indicated establishment after the known date of the wildfire, with 80% of trees having ring counts 2–20 years post-fire, confirming trees were from a similarly-aged post-fire cohort, and not residual from before the fire.

Most C pool sampling occurred during June/July of 2015–2017 within or adjacent to three 30m long plots located ~ 30 m apart within each stand (Appendix 1). To ensure we captured a representative sample of trees within a plot, we used a variable-width belt transect, with width varying between 1 m in high density stands and 8 m in low density stands (30 and 240 m^2). Various other ecological parameters have been described across portions of this gradient using some or all of the stands considered here: understory composition and diversity (Paulson and others 2021), shrub and tree contribution to leaf area (Bendavid and others 2023), stand and tree-level productivity (Walker and others 2021), nitrogen cycling (Hewitt and others 2022a), mycorrhizal and root characteristics (Hewitt and others 2022b), and plant-water relations (Kropp and others 2019). Additional images depicting tree and understory vegetation changes across the density gradient are presented in Paulson and others (2021) and Bendavid and others (2023).

Aboveground C Pools

Within each plot, we inventoried larch trees and tall shrubs (*Salix*, *Betula*, and *Alnus* spp.) and estimated their aboveground biomass using region-specific allometric equations (Alexander and others 2012a; Berner and others 2015). Diameter at breast height (DBH; ≥ 1.4 m tall) or basal diameter (BD; < 1.4 m tall) was measured for each live and dead (that is, snag) larch tree within each plot, and tall shrub BD was measured within a 5–10 m^2 subplot (larger area for lower density) located near plot center. Live larch tree aboveground biomass was converted to C pools by multiplying biomass by 46% C for foliage, 47% C for stemwood/bark, and 48% C for branches (Alexander and others 2012a). Tall shrub biomass was converted to C pools by multiplying by 47% based on average values for all tissue types for similar species in Alaska (Alexander and Mack 2016). Tree inventory of one stand occurred in 2010 as part of another study (Alexander and others 2012a), when a series of five 1 × 20 m belt transects were used to sample trees.

For understory vegetation other than tall shrubs, we determined biomass by harvesting vegetation within a 0.25 m^2 sub-plot located ~ 1 m away from the edge of one randomly-chosen plot in each stand. Only one plot was harvested due to time constraints and the intensive sampling required to sort and dry vegetation with a limited field season. All understory vegetation was harvested down to the top of the soil organic layer (that is, bottom of green moss or top of leaf litter). Vegetation was sorted to the species level, except for graminoids, which were grouped together. All vegetation and litter were dried at 60 °C and their dry weight converted to C by multiplying the dry weight by 50%. Species were later reclassified into plant functional types: forbs, graminoids, mosses, lichens, and short shrubs.

Snag C pools were computed as the difference between total live larch aboveground biomass and live larch crown biomass estimated with allometric equations, and downed woody debris C pools were estimated using the line intercept method (Brown and others 1974). Along the center of each 30 m plot, Class I (0.0–0.49 cm in diameter) and II (0.5–0.99 cm) pieces of fine woody debris (FWD) were tallied along the first 5 m, Class III (1.0–2.99 cm) along the first 10 m, and classes IV (3.0–4.99 cm), V (5.0–6.99 cm), and downed coarse woody debris (CWD; > 7 cm diameter) along the entire 30-m length. Trees were considered CWD and not snags if they were at an angle < 45° to the forest floor. Diameter and decay class of CWD were recorded according to (Manies and others 2005). FWD data were converted to wood mass per unit area using average multiplier values for softwood boreal trees from the Northwest Territories of Canada (Nalder and others 1997). CWD data were converted to mass per unit area using decay classes and density values derived for softwood boreal tree species within Ontario, Canada (Ter-Mikaelian and others 2008). This approach for woody debris biomass was used in a previous study (Alexander and others 2012a) and is maintained here for consistency among our studies and comparison purposes, although we acknowledge that new region-specific woody debris variables are now available (Delcourt and Veraverbeke 2022). Mass values were converted to C pools using 47% C based on that of *L. cajanderi* boles.

Belowground C Pools

We quantified coarse (≥ 2 mm) and fine (< 2 mm) root C pools within each stand by excavating soils. Coarse roots were excavated using a soil saw within a 0.04 m^2 area located ~ 1 m away from the 0 and 30 m locations of plots 1 and 3 in each stand (n = 2/stand). The depth of coarse root sampling varied depending on the depth to which coarse roots were found but never exceeded 21 cm and included the entire organic horizon and the top 1–3 cm of mineral soil. Organic material and/or mineral soil were removed from coarse roots by gently washing under running water. Live coarse roots (determined by tensile strength and color)

were sorted by type (larch or other) and dried at 60 °C to a constant weight. Fine roots were obtained for both the OM (variable depth) and the top 30 cm of the mineral soil at 10 cm depth intervals at the same locations sampled for coarse roots. Fine roots in the OM were obtained from a subsample (~ 10 cm length × 10 cm width) of the soil sample obtained for coarse roots. Fine roots in the OM were carefully removed with tweezers from organic material and gently rinsed with water to remove debris. Fine roots in the mineral soil were collected at 10 cm intervals down to 30 cm from the ground surface (when possible) using a metal corer (6.5 cm diameter). On occasion, frozen soils prevented sampling fine roots in the mineral soil from 20 to 30 cm depth. Live roots in the mineral horizons were cleaned of soil using running water and sieves (2 mm mesh stacked on top of 0.5 mm mesh). Live fine roots were separated from dead ones using the same criteria as coarse roots and dried at 60 °C to a constant weight; roots of different vegetation were not distinguished for fine roots. Coarse and fine root C pools were calculated by dividing the dry mass of the roots by the soil volume sampled and multiplying by depth and then by 50%.

To estimate soil C pools, we sampled OM and near surface mineral soils (30 cm depth) within each stand during 2015, 2016, or 2017. We initially sampled the OM near the 0 and 30 m locations of each sampling plot (n = 6/stand for 16 stands), but because of time constraints in our short field season, we later switched to only sampling soils near plots 1 and 3 (n = 4/stand for 9 stands). Soil OM was sampled with a soil saw, and length, width, and depth recorded from the bottom of the green moss (if present) or top of the leaf litter layer to the top of the mineral soil. Mineral soils were sampled at the same depth intervals using the same methods as described above for fine roots.

Following homogenization and removal of coarse materials (≥ 2 mm), soil subsamples (which included fine roots) were dried at 60 °C (OM) or 105 °C (mineral soil) for 48 h to determine bulk density and soil moisture. Soil C pool values were later corrected by subtracting fine root C pool values. Organic matter content was estimated on oven-dried subsamples by loss-on-ignition (LOI) at 500 °C for 4 h and converted to C content using a linear equation of the relationship between LOI and C content (Alexander and others 2012a). Total C contained within organic and mineral horizons was calculated as the product of each soil core's horizon depth, bulk density, and calculated C content.

Statistical Analyses

We analyzed variations in each C pool and overall C pools (dependent variables) summed into larger categories (for example, total aboveground C = all live aboveground larch C + understory vegetation aboveground C + detrital C; total belowground C = all root C + all soil C; total C = total aboveground C + total belowground C) as a function of tree density (independent variable) using two approaches: (1) fitting linear or linear mixed models that treated each mean C pool at the plot-level or stand-level (when applicable) as a continuous variable, and (2) analyzing C pools at the stand-level as a function of distinct tree density categories based on our previous work in the same fire perimeter (for example, Paulson and others 2021) as well as experimental work testing soil burn severity effects on larch recruitment densities (Alexander and others 2018). We chose to present both approaches for several reasons. The modeling of continuous data provides equations which can be used by others to predict C trajectories with increasing larch tree density, while the categorical data are a useful complement to the modeling analysis, especially in cases where trends are nonlinear and/or data needed to be transformed to meet model assumptions. When on a few occasions the approaches yielded slightly different results, we note that in the results.

For the first approach, we explored C pool patterns across the tree density gradient using linear or linear mixed models that treated C pools as continuous variables. Models were fit to plot-level data across all stands with stand included as a random effect (linear mixed model) for all C pools except forb, graminoid, lichen, moss, and short shrub C pools and total aboveground and overall C pools, which were modeled with stand level data (linear model) because we only had one data point per stand for these variables. While our sampling occurred across several years (2010–2017), most sampling occurred between 2015 and 2017. We were not able to test for an effect of time on C accumulation because sampling year was conflated with tree density. For instance, most low and medium density plots were sampled in 2014/2015, while many high-density plots were sampled in 2017. Nevertheless, rates of C accumulation and change in these systems are very slow (Alexander and others 2012a), and most C pools are unlikely to exhibit year-to-year variability due to background weather conditions, except for herbaceous understory vegetation that represents a very minor C component. When analyzed using plot-level data,

the number of data available for modeling varied between pools because we did not always sample at all three plots each stand for some C pools. For example, roots and soils were sampled in only 2 plots in some stands, and sometimes unthawed permafrost prevented sampling, leading to fewer than 50 plot-level data points for belowground C pools. During analyses, we checked residuals for homogeneity and normality and used a logarithmic or square root transformation of the response variable (denoted in Table 1) to improve homogeneity of variance when needed. For each independent variable, we compared linear, quadratic, and logarithmic models to determine which model was best for each response variable using AICc values. For whichever model provided the best fit (lowest AICc and no problematic patterns in the residuals), we provide goodness of fit information and model parameters (Table 1), but only show regression lines and confidence intervals on figures for the best-fit model when significant ($p_{adj} < 0.05$). We fit a total of 93 models (31 variables each fit with linear, logarithmic, and quadratic fits; all shown in Appendix 4), and adjusted p values using the Benjamini–Hochberg procedure due to multiple testing and report both the modeled and adjusted p values. We also coded each plot or stand data point on the figures by the density categories (described below) used in approach 2. All models were fit using the lme4 package (Bates and others 2015) in R version 4.3.2 (R Core Team 2023).

For the second approach, we subdivided the stands into four density categories according to Paulson and others (2021): low ($n = 5$; < 0.35 stems m^{-2}), medium ($n = 8$; ≥ 0.35 and < 1.0 stems m^{-2}), high ($n = 6$; ≥ 1.0 and < 2.0 stems m^{-2}), and very high ($n = 6$; ≥ 2.0 stems m^{-2}) and tested for significant differences ($p < 0.10$) in mean C pools at the stand level among tree density categories using an ANOVA (JMP v 14.2). We chose to use a higher cutoff for significance because of the relatively small sample size of each density category ($n = 5$–8). All response variables were tested for normality and homogeneity of variance prior to analyses, and when necessary, were transformed using log + 1 or square root transformations to improve adherence to model assumptions. When significant differences ($p < 0.10$) between density categories were found, we conducted a Fisher's LSD post-hoc test comparing means. The data used in this study are available at the Arctic Data Center (Alexander and others 2021a, 2021b, 2024a, 2024b, 2024c).

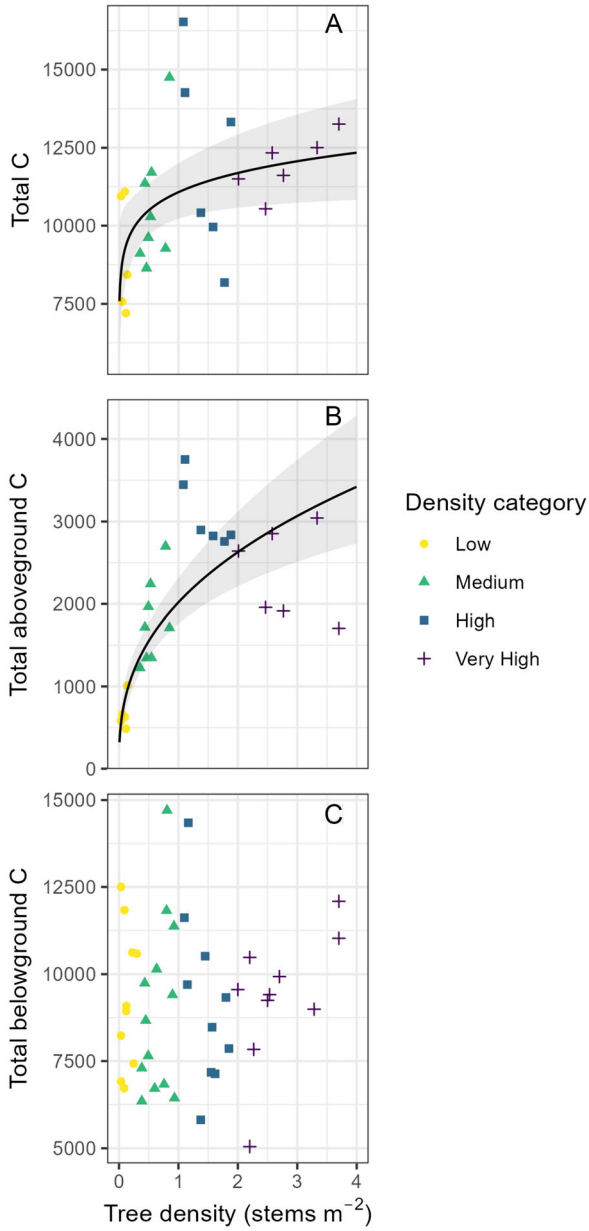

Figure 2. Mean carbon (C; g C m^{-2}) stored in **A** total carbon pools (includes all aboveground + all belowground C pools), **B** total aboveground C pools (includes larch total live aboveground biomass + total understory vegetation biomass + total detrital C pools), and **C** total belowground C pools (includes fine and coarse roots + soil organic matter + and near-surface (30 cm depth) mineral soils), across the post-fire Cajander larch (*Larix cajanderi*) tree density gradient in northeast Siberia. Different colored and shaped symbols represent the mean stand-level (25 stands for total and aboveground C) or plot-level (43 plots for belowground C) observed values across different tree density categories. Solid lines indicate a significant effect (p value < 0.05) of tree density on a given C pool when analyzed as a continuous variable.

Table 1. Summary of Best Fit Models to Predict Carbon Pools (g C m^{-2}) Across the Post-fire Cajander Larch (*Larix cajanderi*) Tree Density Gradient in Northeast Siberia

Carbon Pool	Best fit model type	Conditional R^2	Marginal R^2	*p* value (Satter)	*p* value (adj)	Intercept Coeff (SE)	Tree Dens Coeff (SE)	Tree Dens^2 Coeff (SE)
[1]Total C	logarithmic	0.24	0.21	0.012	**0.036**	9.31 (0.04)	0.08 (0.03)	NA
Live Aboveground Larch								
[2]Foliage	logarithmic	0.89	0.81	< 0.001	< **0.001**	10.89 (0.29)	2.47 (0.18)	NA
[2]Live branches	logarithmic	0.8	0.6	< 0.001	< **0.001**	23.01 (0.86)	4.36 (0.52)	NA
[2]Stems	logarithmic	0.78	0.55	< 0.001	< **0.001**	26.93 (1.08)	4.90 (0.66)	NA
[2]Total larch	logarithmic	0.8	0.6	< 0.001	< **0.001**	37.08 (1.40)	7.00 (0.85)	NA
Understory								
[2] Forb	logarithmic	0.04	0.00	0.352	0.555	2.27 (0.28)	− 0.16 (0.17)	NA
[2]Graminoid	logarithmic	0.02	-0.02	0.470	0.665	1.60 (0.27)	− 0.12 (0.17)	NA
[2]Lichen	linear	0.11	0.07	0.102	0.186	4.24 (0.76)	− 0.75 (0.44)	NA
[2]Moss	logarithmic	0.24	0.2	0.014	**0.037**	6.55 (0.51)	0.86 (0.32)	NA
[2]Short shrub	quadratic	0.32	0.25	0.015	**0.039**	7.89 (0.60)	− 5.72 (2.99)	7.66 (2.99)
[1]Tall shrub	quadratic	0.71	0.26	0.001	**0.005**	3.60 (0.19)	− 4.42 (1.40)	3.52 (1.11)
[2]Total understory	quadratic	0.38	0.33	0.005	**0.016**	14.20 (0.60)	− 8.96 (2.98)	6.40 (2.98)
Detrital								
[2]Fine woody debris	quadratic	0.63	0.25	0.002	**0.008**	9.64 (0.61)	17.00 (4.69)	− 7.16 (3.69)
[2]Coarse woody debris	logarithmic	0.38	0.11	0.019	**0.047**	7.94 (1.24)	1.96 (0.79)	NA
[3]Larch snags	logarithmic	0.73	0.4	< 0.001	< **0.001**	4.14 (0.45)	1.48 (0.27)	NA
[1]Total detrital	logarithmic	0.53	0.29	< 0.001	< **0.001**	5.76 (0.17)	0.49 (0.11)	NA
[1]Total above-ground	logarithmic	0.72	0.71	< 0.001	< **0.001**	7.61 (0.07)	0.38 (0.05)	NA
Roots								
[1]Larch coarse	logarithmic	0.62	0.3	< 0.001	**0.002**	5.22 (0.14)	0.35 (0.09)	NA
[1]Other coarse	quadratic	0.6	0.37	< 0.001	**0.002**	4.26 (0.15)	− 3.07 (1.04)	3.83 (1.03)
OM fine	linear	0.10	0.00	0.800	0.886	355.43 (38.53)	− 6.43 (25.14)	NA
[2]MS 0–10 cm fine	linear	0.76	0.02	0.472	0.665	16.30 (1.96)	− 0.91 (1.25)	NA
[2]MS 10–20 cm fine	linear	0.54	0.02	0.387	0.601	5.61 (0.68)	0.40 (0.45)	NA
[3]MS 20–30 cm fine	logarithmic	0.38	0.13	0.028	0.066	2.37 (0.24)	0.37 (0.16)	NA
[2]Total roots	logarithmic	0.74	0.03	0.299	0.496	30.67 (1.36)	− 0.88 (0.84)	NA
Soils								
[2]Total OM	logarithmic	0.23	0.01	0.405	0.618	51.98 (1.36)	− 0.74 (0.87)	NA
[1]MS 0–10 cm	linear	0.69	0.01	0.557	0.720	7.54 (0.11)	0.04 (0.07)	NA
[2]MS 10–20 cm	linear	0.66	0.03	0.345	0.553	39.02 (1.97)	1.24 (1.29)	NA

Table 1. continued

Carbon Pool	Best fit model type	Conditional R^2	Marginal R^2	p value (Satter)	p value (adj)	Intercept Coeff (SE)	Tree Dens Coeff (SE)	Tree Dens^2 Coeff (SE)
[2]MS 20–30 cm	logarithmic	0.76	0.03	0.290	0.491	37.68 (1.48)	0.96 (0.89)	NA
[1]Total MS	linear	0.83	0.03	0.330	0.538	8.45 (0.09)	0.06 (0.06)	NA
[1]Total soil	linear	0.61	0.01	0.506	0.690	8.93 (0.07)	0.03 (0.04)	NA
[1]Total belowground	linear	0.64	0.01	0.646	0.784	9.06 (0.07)	0.02 (0.04)	NA

NA = not applicable, SE = Standard Error.
Significant models at p value < 0.05 are shown in bold. Data transformations prior to analyses are denoted with superscripts (1 = log, 2 = sqrt, 3 = log + 0.01).

Results

Total C pools increased with increasing larch tree density (Fig. 2a; Table 2), from a mean based on density categories of 8,732 ± 587 g C m^{-2} in low density stands to ~ 11,000 g C m^{-2} in high and very high density stands ($p = 0.07$ across density categories). The best-fit model using the continuous dataset was logarithmic ($p = 0.036$; Table 1; Fig. 2a), with the most pronounced increases occurring at tree densities < 1 stem m^{-2}. Increases in total aboveground C pools drove this trend ($p < 0.001$; Fig. 2b; Table 1; Table 2), as total belowground C pools exhibited no obvious variation with tree density when analyzed either continuously (Fig. 2c; Table 1) or categorically (Table 2).

Live (foliage, leaves, stems, and coarse roots) and detrital (woody debris and snags) larch biomass were the primary contributors to increased total C pools (Fig. 3; Appendix 2). When modeled as a continuous dataset, total C stored in larch aboveground biomass increased logarithmically ($p < 0.001$; Table 1) with increasing tree density (Fig. 3a), similar to total C pools, a pattern also detected for each component (foliage, branches, stems) of larch aboveground biomass (Appendix 2a–c). When considered categorically, total larch aboveground C pools increased ~ tenfold from low (261 ± 91 g C m^{-2}) to high density (2178 ± 144 g C m^{-2}) then declined slightly at very high density (1636 ± 141 g C m^{-2}) ($p < 0.001$ among categories; Table 2). Most C stored aboveground in live larch trees was in stem biomass (~ 55%), with 38% in branches and 6–8% in foliage (Table 2). Belowground larch biomass (that is, coarse roots) also contributed to increasing total C pools with increased tree density (Fig. 3c). Again, the pattern of increase was logarithmic ($p = 0.002$; Table 1), and when compared by density category, there was ~ 2–3 times more larch coarse root C pools in high (337 ± 98 g C m^{-2}) and very high (268 ± 62 g C m^{-2}) density stands compared to low density (124 ± 69 g C m^{-2}) stands ($p = 0.019$ across categories). Total detrital C (CWD, FWD, and snags) also increased logarithmically ($p < 0.001$; Table 1; Fig. 3e) with increasing tree density, with mean values by density category highest in high (768 ± 115 g C m^{-2}) and very high density (573 ± 128 g C m^{-2}) stands and lowest in low density stands (114 ± 31 g C m^{-2}) ($p = 0.005$ across categories). Patterns were generally similar for detrital pools considered individually (Appendix 2j–l; Tables 1, 2).

Table 2. Mean (± SE) Carbon (g C m^{-2}) Pools by Tree Density Category Across the Post-fire Cajander Larch (*Larix cajanderi*) Tree Density Gradient in Northeast Siberia and Results of the ANOVA Test for a Density Category Effect

Carbon Pool (g C m^{-2})	Density category				
	Low	Medium	High	Very High	*p* value
Total Carbon Pools	8732	9940ab	11427ab	11307b	*0.071*
	(587)	(671)	(1108)	(385)	
Aboveground Carbon Pools					
Larch					
Foliage	15c	78b	175a	174a	< **0.001**
	(4)	(10)	(7)	(12)	
Live branches	99d	426c	838a	631b	< **0.001**
	(34)	(58)	(55)	(54)	
Stems	147c	606b	1164a	831b	< **0.001**
	(54)	(86)	(84)	(75)	
Total	261d	1111c	2178a	1636b	< **0.001**
	(91)	(153)	(144)	(141)	
Understory					
Forb	13a	3b	2b	8ab	**0.025**
	(6)	(1)	(1)	(3)	
Graminoids	9a	1c	2bc	6ab	*0.059*
	(6)	(1)	(1)	(3)	
Moss	29	39	60	52	0.241
	(15)	(12)	(13)	(9)	
Lichen	26a	29a	4b	9ab	*0.088*
	(15)	(11)	(2)	(3)	
Short shrub	112a	104a	30b	46ab	**0.033**
	(30)	(26)	(11)	(7)	
Tall shrub	109a	93ab	42bc	20c	**0.001**
	(21)	(15)	(14)	(8.3)	
Total understory	299a	269a	139b	142b	**0.003**
	(33)	(35)	(35)	(12)	
Total live aboveground	559c	1380b	2317a	1777b	< **0.001**
	(107)	(126)	(146)	(134)	
Detrital					
Fine woody debris	39b	92b	186a	109b	**0.007**
	(5)	(18)	(41)	(22)	
Coarse woody debris	22b	48b	198ab	236a	**0.013**
	(9)	(20)	(94)	(83)	
Total woody debris	61b	140b	385a	345a	**0.009**
	(10)	(29)	(111)	(78)	
Larch snags	53b	263a	384a	228a	**0.009**
	(32)	(90)	(67)	(89)	
Total detrital	114c	402bc	768a	573ab	**0.005**
	(31)	(110)	(115)	(128)	
Total aboveground	673d	1782b	3085a	2350b	< **0.001**
	(89)	(178)	(168)	(228)	
Belowground Carbon Pools					
Roots					
Larch coarse	124b	159ab	337a	268a	**0.019**
	(69)	(26)	(98)	(62)	
Other coarse	227a	129b	54c	64bc	**0.001**
	(39)	(25)	(15)	(21)	
Total coarse	351	288	391	332	0.735
	(55)	(34)	(108)	(68)	
OM fine	331	376	351	321	0.874
	(78)	(52)	(36)	(46)	

Table 2. continued

Carbon Pool (g C m^{-2})	Density category				
	Low	Medium	High	Very High	*p* value
MS 0–10 cm fine	365 (158)	254 (47)	393 (207)	162 (23)	0.547
MS 10–20 cm fine	40 (13)	30 (6)	66 (16)	40 (12)	0.178
MS 20–30 cm fine	10 (3)	13 (3)	18.9 (3)	15 (4)	0.333
Total fine	746 (158)	673 (56)	829 (236)	538 (64)	0.522
Total roots	1097 (192)	961 (56)	1220 (339)	869 (96)	0.592
Soils					
Total OM	2466 (232)	2783 (222)	2049 (239)	2399 (445)	0.357
MS 0–10 cm	1587 (99)	1643 (211)	1851 (446)	2286 (232)	0.319
MS 10–20 cm	1608 (169)	1451 (230)	1618 (260)	1964 (136)	0.388
MS 20–30 cm	1300 (188)	1319 (231)	1603 (257)	1439 (117)	0.750
Total MS	4495 (322)	4414 (594)	5073 (878)	5689 (359)	0.434
Total soil	6961 (512)	7196 (680)	7122 (789)	8088 (532)	0.658
Total belowground	8058 (597)	8158 (701)	8342 (983)	8957 (497)	0.834

Significant differences among categories at p value < 0.05 are shown in bold, while those < 0.10 are italicized
SE standard error

As C stored in larch biomass increased, total understory vegetation C pools and coarse roots (that is, ''other'' coarse roots) declined (Fig. 3b and d; Table 2). A quadratic model fitted to continuous data of these pools with tree density provided the best fit (p = 0.016 and 0.002, respectively) (Table 1; Fig. 3b and d). Based on density categories, these pools decreased from low (299 ± 33 and 227 ± 39 g C m^{-2}, respectively) to high (139 ± 35 and 54 ± 15 g C m^{-2}, respectively) density, then remained similarly low at very high density. Trends were driven mostly by changes in tall and short shrub C pools (Appendix 2; Table 2), which comprised 20–40% of total understory aboveground C pools based on density categories (Table 2). Tall and short shrub C pools also exhibited significant quadratic trends (p = 0.005 and 0.039, respectively; Table 1; Appendix 2d–e)) with increasing tree density similar to total understory vegetation. Moss C pools tended to follow larch aboveground C pools, displaying a significant logarithmic trend (p = 0.024; Table 1; Appendix 2f) with increasing tree density, and based on density categories, stored more C in high and very high (~ 50–60 g C m^{-2}) density stands compared to those of low and medium density, although these differences across categories were not significant (p = 0.241; Table 2). Forbs, graminoids, and lichens represented relatively small C pools (means by density category < 30 g C m^{-2} in each pool) and did not display significant linear or curvilinear patterns in C pools with tree density when considered as a continuous dataset (Table 1; Appendix 2 g–i), yet all exhibited significant trends by tree density category, with mean C pools typically highest in low-density stands (Table 2). Despite total understory C pools generally exhibiting an opposite trend to larch aboveground C pools, the increase in total understory C pools with decreasing tree density was insufficient to offset the decrease in larch aboveground C pools (Table 2).

We observed no detectable patterns in OM, near-surface (30 cm depth) MS, or fine root C pools with tree density when analyzed either continuously

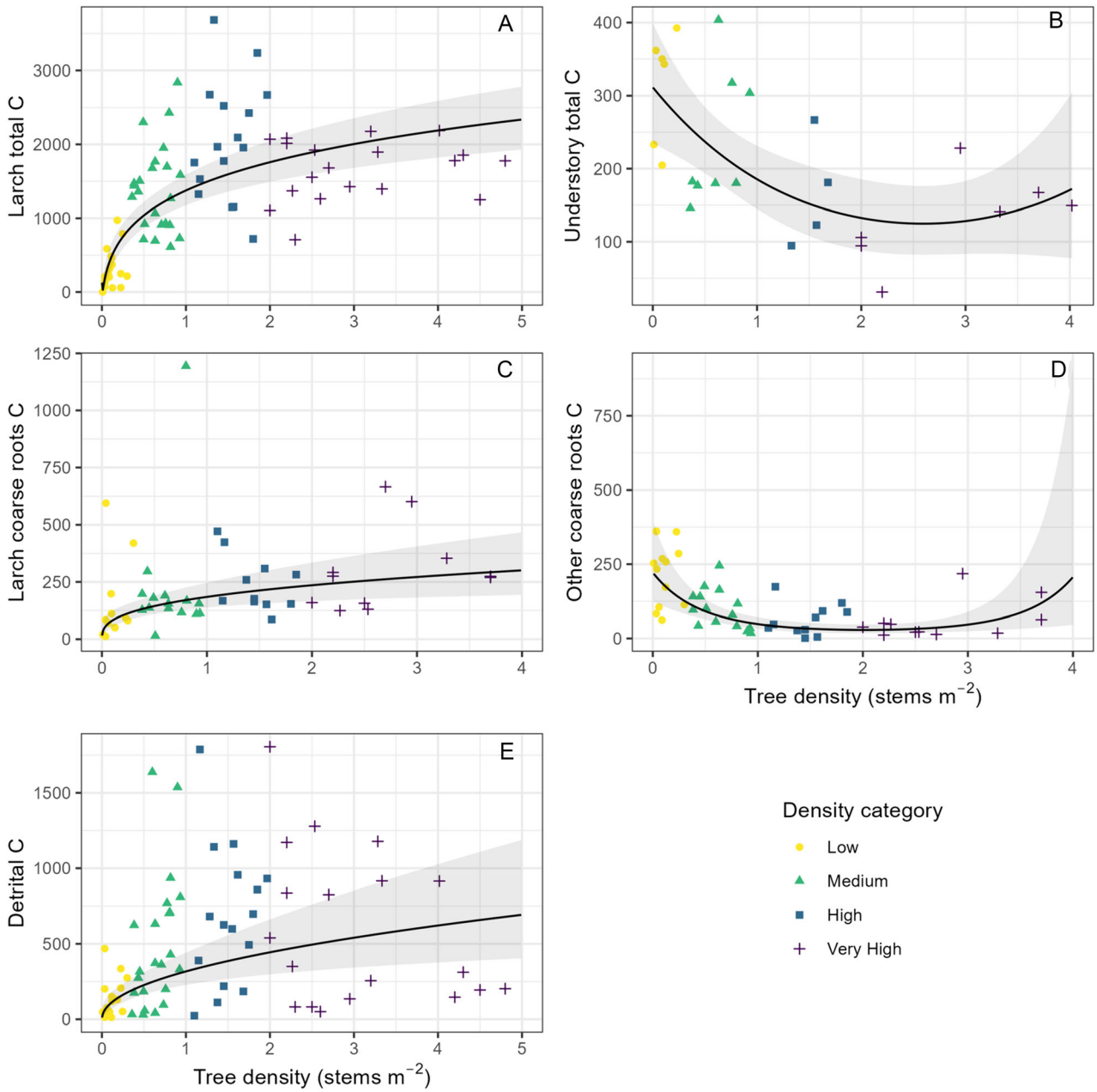

Figure 3. Mean carbon (C; g C m^{-2}) stored in **A** larch total live aboveground biomass, **B** total understory vegetation biomass, **C** larch coarse roots, **D** other vegetation (that is, non-larch) coarse roots, **E** total detrital biomass (includes fine woody debris + coarse woody debris + snags). Different colored and shaped symbols represent the mean plot-level (77 plots) observed values across different tree density categories for all C pools except total understory vegetation, which represent a single value from the one harvested quadrat in each stand (25 stands). Solid lines indicate a significant effect (adj p value < 0.05) of tree density on a given C pool when analyzed as a continuous variable.

(Table 1; Appendix 3) or categorically (Table 2), although we did observe some other important trends. Mean OM C pools, which varied between 2,049 and 2,783 g C m^{-2} across the density categories, represented ~ 18 to 28% of total C pools (Table 2). Mean near-surface MS C pools were relatively evenly distributed between the different depth horizons in all density categories, with ~ 1.5 to 2.5 times as much C stored in the top 30 cm of MS (~ 4,500 to 5,700 g C m^{-2}) compared to soil OM (Table 2). Mean total MS C pools represented ~ 44 to 51% of total C pools (Table 2). Fine

root C pools, which varied between ~ 538 and 829 g C m^{-2} across the mean density categories, declined with depth in the soil profile, with ~ 90% of all fine roots located in the OM and top 10 cm of the MS (Table 2). Based on density categories, most C stored (~ 7,000 to 8,000 g C m^{-2}) in these stands (70–80%) was belowground in OM and near surface (top 30 cm) mineral soils (Table 2).

Discussion

Tree Density in Relation to C Pools

Our findings indicate that processes that impact post-fire larch tree recruitment can ultimately unfold to influence long-term tree density and C storage as stands mature. Most notably, we found that C stored in live larch trees, both in aboveground components and belowground in coarse roots, increased logarithmically with increased tree density, with less pronounced increases above a threshold density (~ 1 stem m^{-2}), likely reflecting limited resources due to increased tree competition. Evaluation of optimal tree densities for Prince Rupprecht's larch (*Larix principis-rupprechtii* Mayr) plantations in northwest China also found that stand volume declined when tree density exceeded 1 stem m^{-2} for stands > 35 year old (Ahmad and others 2018). Snag and woody debris C pools mimicked these trends in larch aboveground biomass, with most dead wood in stands of high and very high density, likely due to shedding of dead wood on lower parts of the tree to maximize leaf area higher in the crown when densely-packed (Gower and Richards 1990) and self-thinning (Pretzsch and others 2023). In previous work, we observed that foliar traits related to C, but not nitrogen (N), changed with increasing tree density, indicating that light limitation, rather than N limitation, is a primary constraint on tree growth in very high density stands (Hewitt and others 2022a), in accordance with larch being a shade-intolerant species (Osawa and others 2010). In addition, although higher density stands had higher stand level aboveground net primary productivity (NPP), they had lower individual tree growth and more negative growth responses to growing season temperature compared to low density stands (Walker and others 2021). Further, individual trees in high density stands produce fewer cones than those in low density stands (Borth and others 2023), again suggesting resource limitation. Nevertheless, larch aboveground C pools in high and very high density stands approximated those previously documented in much older, low density stands (> 200 years) in the same region (Alexander and others 2012a; Webb and others 2017) and in central Siberia (Kajimoto and others 1999), suggesting that increased tree density allows forests to store C faster despite apparent resource limitation at the individual tree level.

Understory vegetation C pools responded to changes in larch dynamics, likely reflecting tree impacts on understory light and/or active layer depth. Moss C pools showed similar logarithmic trends as larch aboveground biomass. Mosses in high-latitude boreal forests are often moisture-limited (Turetsky and others 2012); thus, mosses were likely capitalizing on the likely cooler, moister conditions provided by denser canopies (Hart and Chen 2008) and permafrost thaw water and/or a perched water table associated with shallower active layer in high and very-high density stands. At these sites, canopy cover increased from 13.6% in low density stands to a peak of 70.2% in high density stands, declining slightly to 62.4% in very high density stands, and active layer depth declined from 78.2 cm in low density stands to ~ 50 cm in medium to very high density stands (Paulson and others 2021). Lichen C pools, in contrast, exhibited the opposite pattern, in line with previous research showing that lichens are often found growing beneath open canopies and atop soils with thinner organic layers, higher temperatures, and deeper thaw depths than mosses (Loranty and others 2018). Both tall and short shrub C pools increased with decreased tree density, likely both responding and contributing to deeper active layer depths and more rooting volume and nitrogen availability (Schuur and Mack 2018), as previously documented in these stands (Paulson and others 2021; Hewitt and others 2022a), as well as more light availability (Hart and Chen 2008). Although shrub C pools dominated understory vegetation, leading to the highest understory vegetation C pools in low density stands, this increase was insufficient to offset the much higher C pools stored in aboveground larch biomass in high and very high density stands, leading to total live aboveground C pools in low density stands that were 3–4 times lower. In contrast, increased shrub leaf area index (LAI) in low density stands does compensate for lower larch tree LAI (Bendavid and others 2023), suggesting that trade-offs associated with changing tree density vary among stand level traits related to ecosystem function.

Changes in C pools with tree density were mostly restricted to those associated with live and dead vegetation, with little to no observed variations in

OM or near surface (30 cm depth) mineral soil C pools. The shallower active layer depth previously documented in high and very high density stands indicates that shading from trees helps to keep soils cooler in dense stands, at least during the growing season (Kropp and others 2019); dense stands with higher canopy cover and interception may also collect less snow (Loranty and others 2024), leading to cooler soils in the dormant season (Schneider and others 2018). While this shading does not appear to currently impact the total storage of near surface soil C in high density stands compared to lower density stands, the shading effects of high canopy cover on underlying soil conditions could become more important as climate warming continues. Given that soil C pools accounted for 60–80% of total C pools across the tree density gradient, protecting these pools from degradation and subsequent release in the atmosphere is critically important.

Like boreal forests of Western North America, our data show trade-offs in the type, location, and size of C pools with shifts in dominant vegetation functional types following fire, but the impact on whole-ecosystem C storage appears to differ between the regions. In Alaska and Western Canada, for example, black spruce (*Picea mariana* (Mill.) B. S. P.) forests commonly shift to forests dominated by deciduous hardwoods following high severity fire (Baltzer and others 2021), leading to a shift in C storage from predominantly belowground C in thick organic soils in black spruce stands to mostly aboveground C stored in trees of hardwood-dominated stands, but no net change in total ecosystem C storage (Alexander and others 2012b; Alexander and Mack 2016). The shift to deciduous hardwoods has been able to offset C lost during the high severity fires that often trigger this shift in forest ecosystem state (Mack and others 2021). In contrast, in high latitude Siberian larch forests where larch is monodominant, increased fire severity could promote a shift in tree density (Alexander and others 2018), not in tree functional types. Thus, forests may transition from open forests with few trees embedded in a shrub matrix to forests of high tree density and few shrubs. Because trees and shrubs differ in their C storage capacity, and these ecosystem states do not appear to vary in their OM soil C storage, the net effect of increasing tree density is increased total C storage, a pattern that differs from that in Western North America. We do not yet know whether this shift from low to high density stands is sufficient to offset the C lost during the presumably high-severity fires that promote larch recruitment (Alexander and others 2018). Clearly, patterns of post-fire forest C trajectories in high-latitude larch forests differ from those in Western North America, but the balance between C lost during fire and C recovered during the post-fire successional interval still needs to be resolved.

Our study has several limitations that deserve mention. First, our sampling was confined to a single fire perimeter, and relationships between post-fire larch tree density and C pools may vary depending on underlying environmental conditions across the broader landscape where larch forests are found (for example, topography, landscape position, plant community composition, climate) that we could not account for in this study. In addition, due to logistical constraints associated with sampling in a such a remote region (for example, limited field season, difficulty transporting and/or processing soil and vegetation samples from field sites), our sample sizes for harvested material (soils, roots, understory vegetation) are relatively small, which likely contributed to the high variability in C pools even within density categories and sometimes decoupling of patterns when C pools were analyzed as continuous or categorical data. Thus, at high latitudes where larch are monodominant, changes in larch tree density likely correspond to changes in C pools as described here, but these patterns may not always hold true, especially at lower latitudes where larch co-exist with other conifers and deciduous hardwood tree species.

Implications of Tree Density on Ecosystem Processes

Changes in larch tree density are likely to occur across Siberia in response to climate warming through tree migration north into areas previously considered tundra (Kruse and others 2016) and climate-driven modifications to the fire regime (Alexander and others 2018), and these forest structural changes are likely to impact a suite of ecosystem-level processes in addition to C storage. Our previous work on understory plant biodiversity indicated that species abundance and diversity decreased with increased canopy cover associated with increased tree density, likely due to low resource availability (Paulson and others 2021), a trend also observed in Dahurian larch *(Larix gmelinii* (Rupr.) Rupr.) forests (Ma and others 2016). Open forests with more shrubs have higher winter albedos and increased snow accumulation compared to more dense stands, leading to warmer summer and winter soil temperatures (Loranty and others 2021, 2024). High density stands tend to

transpire more water and have greater canopy stomatal conductance relative to low density stands during wet portions of the growing season, indicating a stronger dependence on past precipitation events (Kropp and others 2019), and increasing larch density accelerates stand level nitrogen cycling (Hewitt and others 2022a). Thus, stand density impacts more than C storage, with implications for biodiversity, surface energy dynamics, water cycling, and nutrient cycling.

Ultimately, the prevalence and persistence of high density larch stands across the region depend on the interplay of factors that impact initial recruitment patterns (that is, seed availability, seedbed quality, competition) and competition between individual trees as stands mature, which could alter density through self-thinning, and susceptibility to future fires. As fire extent continues to increase in area throughout the region (Talucci and others 2022a), seed availability within interior portions of fire perimeters is likely to decline, leading to forest loss and/or low density stands. Increased fire frequency is also likely to reduce seed availability by decreasing tree age, thus time to reach maturity and bear seeds. However, increased soil burn severity and improved seedbed conditions along the burn perimeter could create zones of high density stands, especially if fires occur just before a mast year, as these areas are adjacent to nearby seed sources from unburned trees. Once high density stands establish, there are likely to be feedbacks to future fire regimes. High foliar moisture of larch may decrease ignitability of high density stands (Rogers and others 2015), but in dry conditions, more densely-packed trees could facilitate crown fires because flames more easily spread from one tree to the next when tree crowns are connected (Kharuk and others 2021). If fires in densely-packed stands are concentrated in tree crowns, rather than on the soil surface, this could help to limit soil OM carbon loss, as 25–30% of total soil C pools are stored in the OM, which is often a primary fuel in surface fires (Alexander and others 2018). However, fires in densely-packed stands could move through both the crowns and surface soils, increasing vulnerability of both aboveground and surface soil C pools. If pest or pathogen outbreaks increase in relation to climate change, as noted in forests across the U.S.A (Kolb and others 2016), outbreak spread would be greater in closely-packed, dense stands, which also could interact with fire behavior to impact fire frequency (Kharuk and Antamoshkina 2017). In the absence of fire effects, the persistence of high density stands depends largely on self-thinning processes, which could gradually reduce larch density and the relative proportion of C stored in living versus detrital biomass (that is, snags and woody debris). However, self-thinning does not always occur. Even in very high density stands, stagnation can occur, leading to little changes in stand density and individual tree size as stands age (Alexander and others 2012a). Thus, understanding multiple ecosystem-level impacts of varying tree demography, especially in monodominant larch forests that currently occupy vast areas of Eastern Siberia and are experiencing increased fire activity, is critically important for predicting future feedbacks between high-latitude forests and regional climate.

Conclusions

In mature, relatively even-aged larch stands that regenerated following a stand-replacing fire $\sim$ 75 years ago, total C pools increased with increased larch density, largely due to increased larch aboveground and coarse root C pools, as total understory vegetation C pools declined with increased tree density and OM and near surface (30 cm depth) MS C pools were relatively similar across the density gradient. Our previous work showed that increased tree density also corresponded with higher canopy cover, cooler surface soils, and shallower active layer depths. In addition to storing more C, high density stands could create a more stable understory environment for underlying permafrost soils, although this could change if more densely-stocked stands become more susceptible to fire or start to self-thin as they continue to age. Our findings highlight the potential for a climate-driven increase in fire severity to alter tree recruitment, successional dynamics, and C cycling in Siberian larch forests. Consequently, factors that impact tree density early in forest succession are likely to have long-term impacts on overall forest function throughout the successional interval.

Acknowledgements

This project was supported by funding from the National Science Foundation (PLR-1304040, PLR-1623764, PLR-1304007, PLR-1303940, OISE-1032373; Alexander, Loranty, Natali, Mack). We thank L. Berner, P. Ganzlin, B.J. Petronio-Nyberg, A. White, E. Ramos, J. McMahon, P. Watson, M. Boyd, E. Babl-Plauche, B. Izbicki, E. Borth, and R. Hewitt for field and lab assistance, and the staff and scientists at the Northeast Science Station for logistical and field support.

REFERENCES

Abaimov AP. 2010. Geographical distribution and genetics of Siberian larch species. Permafrost Ecosystems, Springer pp 41–58.

Ahmad B, Wang Y, Hao J, Liu Y, Bohnett E, Zhang K. 2018. Optimizing stand structure for trade-offs between overstory timber production and understory plant diversity: a case-study of a larch plantation in northwest China. Land Degr Develop 29:2998–3008.

Alexander HD, Paulson AP, Hewitt R, Loranty M, Mack M, Natali S. 2021a. Larch tree carbon pools across a post-fire tree density gradient in far northeastern Siberia, 2010–2017. Arctic Data Center. https://doi.org/10.18739/A29W09090.

Alexander HD, Paulson AP, Hewitt R, Loranty M, Mack M, Natali S. 2021b. Root carbon pools across a post-fire tree density gradient in far northeastern Siberia, 2015–2017. Arctic Data Center. https://doi.org/10.18739/A2639K644.

Alexander HD, Paulson AP, Loranty M, Natali S, Mack M. 2024a. Organic and near-surface mineral soil carbon pools across a post-fire tree Arctic Data Center density gradient in far northeastern Siberia, 2015–2017. https://doi.org/10.18739/A2CV4BT2K

Alexander HD, Paulson AP, Loranty M, Natali S, Mack M. 2024b. Understory vegetation carbon pools across a post-fire tree density gradient in far northeastern Siberia, 2015-2017. Arctic Data Center. https://doi.org/10.18739/A24B2X66C

Alexander HD, Paulson AP, Loranty M, Natali S, Mack M. 2024c. Woody debris and snag carbon pools across a post-fire tree density gradient in far northeastern Siberia, 2010-2017. Arctic Data Center. https://doi.org/10.18739/A2833N091

Alexander HD, Mack MC. 2016. A canopy shift in interior Alaskan boreal forests: consequences for above – and below-ground carbon and nitrogen pools during post – fire succession. Ecosystems 19(1):98–114.

Alexander HD, Mack MC, Goetz S, Loranty MM, Beck PS, Earl K, Zimov S, Davydov S, Thompson CC. 2012a. Carbon accumulation patterns during post-fire succession in Cajander larch (Larix cajanderi) forests of Siberia. Ecosystems 15:1065–82.

Alexander HD, Mack MC, Goetz S, Beck PSA, Belshe F. 2012b. Implications of increased deciduous cover on stand structure and aboveground carbon pools of Alaskan boreal forests. Ecosphere 3(5):45.

Alexander HD, Natali SM, Loranty MM, Ludwig SM, Spektor VV, Davydov S, Zimov N, Trujillo I, Mack MC. 2018. Impacts of increased soil burn severity on larch forest regeneration on permafrost soils of far northeastern Siberia. For Ecol Manage 417:144–153.

Anjos L, Gaistardo CC, Deckers J, Dondeyne S, Eberhardt E, Gerasimova M, Harms B, Jones A, Krasilnikov P, Reinsch T, Vargas R, Zhang G-L. 2016. World reference base for soil resources: 2014 International soil classification system for naming soils and creating legends for soil maps. JRC Publications Repository.

Baltzer JL, Day NJ, Walker XJ, Greene D, Mack MC, Alexander HD, Arseneault D, Barnes J, Bergeron Y, Boucher Y, Bourgeau-Chavez L. 2021. Increasing fire and the decline of fire adapted black spruce in the boreal forest. Proc Natl Acad Sci 118(45):e202487211.

Bates D, Maechler M, Bolker B, Walker S. 2015. Fitting linear mixed-effects models using lme4. J Stat Softw 67(1):1–48. https://doi.org/10.18637/jss.v067.i01.

Bendavid NS, Alexander HD, Davydov SP, Kropp H, Mack MC, Natali SM, Spawn-Lee SA, Zimov NS, Loranty MM. 2023. Shrubs compensate for tree leaf area variation and influence vegetation indices in post-fire Siberian larch forests. J Geophys Res: Biogeosci 128(3):e2022JG007107.

Berner LT, Alexander HD, Loranty MM, Ganzlin P, Mack MC, Davydov SP, Goetz SJ. 2015. Biomass allometry for alder, dwarf birch, and willow in boreal forest and tundra ecosystems of far northeastern Siberia and north-central Alaska. Forest Ecol Manage 337:110–18.

Berner LT, Beck PSA, Loranty MM, Alexander HD, Mack MC, Goetz SJ. 2012. Cajander larch (*Larix cajanderi*) biomass distribution, fire regime and post-fire recovery in northeastern Siberia. Biogeosciences 9:3943–59.

Borth EB, Alexander HD, Zimov N, McEwan RW. 2023. Seed sources and safe sites as drivers of *Larix cajanderi* regeneration following wildfire in the Siberian Arctic. Ecosphere 14:e4617.

Brown CD, Liu J, Yan G, Johnstone JF. 2015. Disentangling legacy effects from environmental filters of postfire assembly of boreal tree assemblages. Ecology 96:3023–32.

Brown JK, others. 1974. Handbook for inventorying downed woody material. USDA Forest Service General Technical Report INT-16, 32.

Cai W, Yang J, Liu Z, Hu Y, Weisberg PJ. 2013. Post-fire tree recruitment of a boreal larch forest in Northeast China. For Ecol Manage 307:20–9.

Cai WH, Liu Z, Yang YZ, Yang J. 2018. Does environment filtering or seed limitation determine post-fire forest recovery patterns in boreal larch forests? Front Plant Sci 9:1318.

Cai WH, Yang J. 2016. High-severity fire reduces early successional boreal larch forest aboveground productivity by shifting stand density in north-eastern China. Int J Wildland Fire 25:861–75.

Delcourt CJF, Veraverbeke S. 2022. Allometric equations and wood density parameters for estimating aboveground and woody debris biomass in Cajander larch (*Larix cajanderi*) forests of northeast Siberia. Biogeosciences 19:4499–4520.

Descals A, Gaveau DL, Verger A, Sheil D, Naito D, Peñuelas J. 2022. Unprecedented fire activity above the Arctic Circle linked to rising temperatures. Science 378:532–37.

Fan L, Wigneron J-P, Ciais P, Chave J, Brandt M, Sitch S, Yue C, Bastos A, Li X, Qin Y. 2023. Siberian carbon sink reduced by forest disturbances. Na Geosci 16:56–62.

Fedorov-Davydov D, Davydov S, Davydova A, Shmelev DG, Ostroumov VE, Kholodov A, Sorokovikov VA. 2018. The thermal state of soils in northern Yakutia. Earth's Cryosphere XXII:47–58.

Furyaev VV, Vaganov EA, Tchebakova NM, Valendik EN. 2001. Effects of fire and climate on successions and structural changes in the Siberian boreal. Eurasian J For Res 2:1–15.

Gower ST, Richards JH. 1990. Larches: deciduous conifers in an evergreen world. BioScience 40:818–26.

Hart SA, Chen HY. 2008. Fire, logging, and overstory affect understory abundance, diversity, and composition in boreal forest. Ecol Monogr 78:123–140.

Hewitt RE, Alexander HD, Izbicki B, Loranty MM, Natali SM, Walker XJ, Mack MC. 2022a. Increasing tree density accelerates stand-level nitrogen cycling at the taiga–tundra ecotone in northeastern Siberia. Ecosphere 13:e4175.

Hewitt RE, Alexander HD, Miller SN, Mack MC. 2022b. Root-associated fungi not tree density influences stand nitrogen dynamics at the larch forest–tundra ecotone. J Ecol 110:1419–31.

Hewitt RE, Day NJ, DeVan MR, Taylor DL. 2022c. Wildfire impacts on root-associated fungi and predicted plant–soil feedbacks in the boreal forest: research progress and recommendations. Funct Ecol 37(8):2110–25.

Holloway JE, Lewkowicz AG, Douglas TA, Li X, Turetsky MR, Baltzer JL, Jin H. 2020. Impact of wildfire on permafrost landscapes: a review of recent advances and future prospects. Permafrost Periglacial Process 31:371–82.

Johnstone JF, Chapin FS III. 2006. Effects of soil burn severity on post-fire tree recruitment in boreal forest. Ecosystems 9:14–31.

Kajimoto T, Matsuura Y, Sofronov MA, Volokitina AV, Mori S, Osawa A, Abaimov AP. 1999. Above-and belowground biomass and net primary productivity of a *Larix gmelinii* stand near Tura, central Siberia. Physiol 19:815–22.

Kasischke ES, Stocks BJ. 2012. Fire, climate change, and carbon cycling in the boreal forest. Vol. 138. Springer Science & Business Media.

Kharuk VI, Antamoshkina OA. 2017. Impact of silkmoth outbreak on taiga wildfires. Contemp Probl Ecol 10:556–62.

Kharuk VI, Ponomarev EI, Ivanova GA, Dvinskaya ML, Coogan SC, Flannigan MD. 2021. Wildfires in the Siberian taiga. Ambio:1–22.

Kharuk VI, Ranson KJ, Dvinskaya ML. 2010. Wildfire dynamics in mid-Siberian larch dominated forests. In: Environmental Change in Siberia. Springer. pp 83–100.

Kharuk VI, Ranson KJ, Dvinskaya ML, Im ST. 2011. Wildfires in northern Siberian larch dominated communities. Environ Res Lett 6:045208.

Kirdyanov AV, Saurer M, Siegwolf R, Knorre AA, Prokushkin AS, Churakova OV, Fonti MV, Büntgen U. 2020. Long-term ecological consequences of forest fires in the continuous permafrost zone of Siberia. Environ Res Lett 15:034061.

Kobak KI, Turcmnovich IY, Kondrasiheva NY, Schulze E-D, Schulze W, Koch H, Vygodskaya NN. 1996. Vulnerability and adaptation of the larch forest in eastern Siberia to climate change. Water Air Soil Pollut 92:119–27.

Kolb TE, Fettig CJ, Ayres MP, Bentz BJ, Hicke JA, Mathiasen R, Stewart JE, Weed AS. 2016. Observed and anticipated impacts of drought on forest insects and diseases in the United States. For Ecol Manage 380:321–34.

Kropp H, Loranty MM, Natali SM, Kholodov AL, Alexander HD, Zimov NS, Mack MC, Spawn SA. 2019. Tree density influences ecohydrological drivers of plant-water relations in a larch boreal forest in Siberia. Ecohydrology 12:e2132.

Kruse S, Wieczorek M, Jeltsch F, Herzschuh U. 2016. Treeline dynamics in Siberia under changing climates as inferred from an individual-based model for *Larix*. Ecolog Modell 338:101–21.

Krylov A, McCarty JL, Potapov P, Loboda T, Tyukavina A, Turubanova S, Hansen MC. 2014. Remote sensing estimates of stand-replacement fires in Russia, 2002–2011. Environ Res Lett 9:105007.

Loranty MM, Alexander HD, Kropp H, Talucci AC, Webb EE. 2021. Siberian ecosystems as drivers of cryospheric climate feedbacks in the terrestrial Arctic. Front Climate 3:730943.

Loranty MM, Berner LT, Taber ED, Kropp H, Natali SM, Alexander HD, Davydov SP, Zimov NS. 2018. Understory vegetation mediates permafrost active layer dynamics and carbon dioxide fluxes in open-canopy larch forests of northeastern Siberia. PloS One 13:e0194014.

Loranty, M. M., Alexander, H. D., Davydov, Kholodov, A. L., S. P., Kropp, H., M., Mack, Natali, S. M. C., Zimov, N. S. 2024. Winter soil temperature varies with canopy cover in Siberian larch forests. Environmental Research Letters. 19(5):054013.

Loranty MM, Liberman-Cribbin W, Berner LT, Natali SM, Goetz SJ, Alexander HD, Kholodov AL. 2016. Spatial variation in vegetation productivity trends, fire disturbance, and soil carbon across arctic-boreal permafrost ecosystems. Environ Res Lett 11:1–14.

Ma J, Bu R, Liu M, Chang Y, Han F, Qin Q, Hu Y. 2016. Recovery of understory vegetation biomass and biodiversity in burned larch boreal forests in Northeastern China. Scandinavian J For Res 31:382–93.

Mack MC, Walker XJ, Johnstone JF, Alexander HD, Melvin AM, Jean M, Miller SN. 2021. Carbon loss from boreal forest wildfires offset by increased dominance of deciduous trees. Science 372(6539):280–83.

Mack MC, Bret-Harte MS, Hollingsworth TN, Jandt RR, Schuur EA, Shaver GR, Verbyla DL. 2011. Carbon loss from an unprecedented Arctic tundra wildfire. Nature 475:489–92.

Manies KL, Harden JW, Bond-Lamberty BP, O'neill KP. 2005. Woody debris along an upland chronosequence in boreal Manitoba and its impact on long-term carbon storage. Can J Forest Res 35:472–82.

Nalder IA, Wein RW, Alexander ME, de Groot WJ. 1997. Physical properties of dead and downed round-wood fuels in the boreal forests of Alberta and Northwest Territories. Can J For Res 27:1513–17.

Osawa A, Zyryanova OA, Matsuura Y, Kajimoto T, Wein RW. 2010. Permafrost ecosystems: Siberian larch forests. Springer Science & Business Media.

Paulson AK, Peña H III, Alexander HD, Davydov SP, Loranty MM, Mack MC, Natali SM. 2021. Understory plant diversity and composition across a postfire tree density gradient in a Siberian Arctic boreal forest. Can J For Res 51:720–31.

Ponomarev EI, Kharuk VI, Ranson KJ. 2016. Wildfires dynamics in Siberian larch forests. Forests 7:125.

Pretzsch H, del Río M, Arcangeli C, Bielak K, Dudzinska M, Ian Forrester D, Kohnle U, Ledermann T, Matthews R, Nagel R, Ningre F, Nord-Larsen T, Szeligowski H, Biber P. 2023. Competition-based mortality and tree losses. An essential component of net primary productivity. For Ecol Manage 544:121204.

R Core Team. 2023. R: A Language and Environment for Statistical Computing. R Foundation for Statistical Computing, Vienna, Austria. https://www.R-project.org/.

Rogers BM, Soja AJ, Goulden ML, Randerson JT. 2015. Influence of tree species on continental differences in boreal fires and climate feedbacks. Nature Geosci 8:228.

Schaphoff S, Reyer CP, Schepaschenko D, Gerten D, Shvidenko A. 2016. Tamm review: observed and projected climate change impacts on Russia's forests and its carbon balance. Forest Ecol Manage 361:432–44.

Schneider A., Flanner M., De Roo R., Adolph A. 2019. Monitoring of snow surface near-infrared bidirectional reflectance factors with added light-absorbing particles. The Cryosphere, 13(6):1753-1766.

Schuur EAG, Mack MC. 2018. Ecological response to permafrost thaw and consequences for local and global ecosystem services. Ann Rev Ecol Evolut Syst 49:279–301.

Shuman JK, Foster AC, Shugart HH, Hoffman-Hall A, Krylov A, Loboda Tatiana, Ershov D, Sochilova E. 2017. Fire disturbance and climate change: implications for Russian forests. Environ Res Lett 12:035003.

Sofronov MA, Volokitina AV. 2010. Wildfire ecology in continuous permafrost zone. Permafrost Ecosystems: Siberian Larch Forests. pp 59–82.

Stewart JA, van Mantgem PJ, Young DJ, Shive KL, Preisler HK, Das AJ, Stephenson NL, Keeley JE, Safford HD, Wright MC. 2021. Effects of postfire climate and seed availability on postfire conifer regeneration. Ecol Appl 31:e02280.

Strauss J, Schirrmeister L, Grosse G, Fortier D, Hugelius G, Knoblauch C, Romanovsky V, Schädel C, von Deimling TS, Schuur EA. 2017. Deep Yedoma permafrost: a synthesis of depositional characteristics and carbon vulnerability. Earth-Sci Rev 172:75–86.

Talucci AC, Loranty MM, Alexander HD. 2022a. Siberian taiga and tundra fire regimes from 2001–2020. Environ Res Lett 17:025001.

Talucci AC, Loranty MM, Alexander HD. 2022b. Spatial patterns of unburned refugia in Siberian larch forests during the exceptional 2020 fire season. Global Ecol and Biogeogr 00:1-15.

Tchebakova NM, Parfenova E, Soja AJ. 2009. The effects of climate, permafrost and fire on vegetation change in Siberia in a changing climate. Environ Res Lett 4:045013.

Ter-Mikaelian MT, Colombo SJ, Chen J. 2008. Amount of downed woody debris and its prediction using stand characteristics in boreal and mixedwood forests of Ontario, Canada. Can J Forest Res 38:2189–97.

Turetsky MR, Bond-Lamberty B, Euskirchen E, Talbot J, Frolking S, McGuire AD, Tuittila E-S. 2012. The resilience and functional role of moss in boreal and arctic ecosystems. New Phytologist 196:49–67.

Walker XJ, Alexander HD, Berner LT, Boyd MA, Loranty MM, Natali SM, Mack MC. 2021. Positive response of tree productivity to warming is reversed by increased tree density at the Arctic tundra–taiga ecotone. Can J Forest Res 51:1323–38.

Webb EE, Heard K, Natali SM, Bunn AG, Alexander HD, Berner LT, Kholodov A, Loranty MM, Schade JD, Spektor V. 2017. Variability in above-and belowground carbon stocks in a Siberian larch watershed. Biogeosciences 14:4279.

Webb EE, Alexander HD, Paulson AK, Loranty MM, DeMarco J, Talucci AC, Spektor V, Zimov N, Lichstein JW. 2024. Carbon loss and tree mortality following fire in Siberian larch forests. Geophys Res Lett 51(1):e2023GL105216.

Witze A. 2020. Why Arctic fires are bad news for climate change. Nature 585:336–37.